Applied Environmental Research (2026) 48(3), 017
https://doi.org/10.35762/AER.2026017

Applied Environmental Research
- RESEARCH FOR SUSTAINABLE PLANET -

Research Article

Bioremediation Potential of Indigenous *Stutzerimonas stutzeri* 08TBb Isolated from Mercury-Contaminated Gold Mining Sites in Indonesia

Uun Rohmawati[1,*], Juanita Hibatullah[2], Achmad Rodiansyah[3], Yunita Messe[4], Dwi Nur Aini Fajriah[1]

[1] *Department of Biology Education, Faculty of Science and Education, Universitas Nahdlatul Ulama Pasuruan, Pasuruan 67171, Indonesia*
[2] *Department of Biology, Faculty of Science and Technology, Universitas Merangin, Jambi 37314, Indonesia*
[3] *Department of Biotechnology, School of Life Sciences and Technology, Institut Teknologi Bandung, Bandung 40132, Indonesia*
[4] *Department of Tropical Biology, Faculty of Biology, Universitas Gadjah Mada, Yogyakarta 55281, Indonesia*

*Corresponding Email: Uun Rohmawati (rohmawati@unupasuruan.ac.id)

Abstract

Artisanal and small-scale gold mining (ASGM) widely uses mercury (Hg) in the amalgamation process, and the resulting waste is often discharged directly into the environment, posing serious risks to ecosystems and human health because of the high toxicity of Hg. This study aimed to isolate and screen indigenous Hg-tolerant bacteria from contaminated gold mining sites in Indonesia; characterize the most effective isolate using morphological, biochemical, and molecular approaches; evaluate Hg(II) degradation performance using ICP–OES, FTIR, and SEM analyses; and identify key metabolites involved in Hg detoxification through untargeted LC–HRMS metabolomics. A total of 51 bacterial isolates were obtained from Hg-contaminated gold mining waste, of which the five isolates showing the smallest inhibition zones at increasing Hg^{2+} concentrations were selected as Hg-resistant candidates. Among these, isolate 08TBb exhibited the most stable growth under high Hg concentrations and was selected for further characterization. Morphological, biochemical, and 16S rRNA gene-based molecular identification revealed that isolate 08TBb shared high similarity (≥99%) with *Stutzerimonas stutzeri*. ICP–OES analysis demonstrated a significant reduction in Hg concentration during bacterial cultivation, indicating effective Hg removal. FTIR analysis revealed that bacterial treatment altered the chemical form of Hg in the medium, suggesting a transition from inorganic Hg–Cl bonds to Hg–biomolecule complexes followed by enzymatic reduction. SEM revealed distinct morphological changes in bacterial cells exposed to Hg, including surface roughening, aggregation, and granular deposits associated with Hg accumulation. Untargeted LC–HRMS metabolomic analysis revealed a distinct metabolic response dominated by sulfur-containing compounds, stress-related amino acids and peptides, osmoprotectants, nucleotides, and membrane-associated lipids, indicating coordinated mechanisms of metal binding, redox regulation, and cellular structural adaptation. Overall, the findings highlight the strong potential of *Stutzerimonas stutzeri* 08TBb as an effective indigenous bacterium for Hg bioremediation.

ARTICLE HISTORY

Received: 15 Dec. 2025
Revised: 21 May 2026
Accepted: 29 May 2026
Published: 8 Jul 2026

KEYWORDS

Biosorption;
Heavy metal remediation;
ICP–OES;
LC–HRMS metabolomics;
Mercury resistance

Introduction

Artisanal and small-scale gold mining (ASGM) remains among the major contributors to mercury (Hg) pollution because Hg is still widely used for gold amalgamation (Telmer and Veiga, 2009). In Indonesia, ASGM activities are widespread, particularly in Jambi

Province, including areas such as Lubuk Gaung, Muara Jernih, and Bukit Bangkul, where Hg continues to be applied in gold extraction processes. After amalgamation occurs, Hg-contaminated tailings are frequently discharged directly into the surrounding environment without pretreatment, resulting in the accumulation of Hg in soils, sediments, and water bodies (Esdaile et al., 2018). This contamination poses serious environmental and public health risks because Hg is persistent, highly toxic, and capable of biomagnification through food chains, thereby threatening ecosystem stability and human well-being (Fioravanti et al., 2025).

Various physical and chemical approaches, including adsorption, precipitation, and chemical reduction, have been applied to remediate Hg-contaminated environments. However, these methods often suffer from high operational costs, limited field applicability, and the generation of secondary waste (Rohmawati et al., 2022; Wang et al., 2020). Consequently, increasing attention has been given to environmentally sustainable and cost-effective remediation technologies, particularly bioremediation, which utilize microorganisms to detoxify, transform, or immobilize pollutants (Pande et al., 2022). Microbial bioremediation offers several advantages because bacteria can function under natural environmental conditions, require minimal chemical inputs, and may function efficiently at large scales.

Bacteria are generally considered more effective bioremediation agents than fungi or algae because they exhibit faster growth rates, greater metabolic flexibility, and stronger physiological resilience when exposed to toxic pollutants (Chakraborty et al., 2025; Kumar et al., 2026). Their versatile catabolic pathways enable rapid pollutant transformation, while many bacterial taxa possess metal resistance systems that allow continued metabolic activity under elevated concentrations of contaminants such as Hg(II) and Pb(II) (Tang et al., 2024). In contrast, fungal remediation often requires longer colonization periods and more complex extracellular enzymatic processes, which may limit rapid responses under fluctuating environmental conditions (Harms et al., 2011). Owing to their adaptability, rapid reproduction, and ability to survive under nutrient-poor and toxic conditions, bacteria, particularly indigenous strains, are regarded as practical and robust microbial agents for field-scale biodegradation and heavy metal bioremediation (Gadd, 2011).

Indigenous bacteria isolated from Hg-contaminated environments are particularly promising because they have undergone long-term evolutionary adaptation to metal stress (Timková et al., 2024). Mercury-resistant bacteria (MRB) commonly employ multiple detoxification mechanisms, including biosorption, bioaccumulation, enzymatic transformation, and modifications of cell-surface functional groups capable of binding Hg(II) (Barkay et al., 2003). Several studies have successfully isolated MRB from mine tailings and demonstrated its ability to remove or detoxify Hg under laboratory conditions (Pushkar et al., 2019). However, despite these advances, a comprehensive understanding of Hg detoxification mechanisms, including structural changes, molecular interactions, and metabolite production, remains limited for many indigenous strains, particularly in Indonesia's ASGM regions.

Several Hg-resistant bacterial species have previously been widely documented for their ability to transform, reduce, or immobilize Hg(II) in contaminated environments, mainly through biosorption, bioaccumulation, and enzymatic transformation. By expressing the enzyme mercuric reductase (MerA), species such as *Pseudomonas putida* and *Pseudomonas aeruginosa* exhibit strong Hg(II) reduction capacity, allowing efficient volatilization of Hg(0) under aerobic conditions, whereas *Cupriavidus metallidurans* MSR33 demonstrates broad-spectrum metal resistance and high Hg(II) detoxification efficiency in both soil and aqueous matrices (Bravo et al., 2020; Pushkar et al., 2019). Several *Bacillus* species, including *Bacillus toyonensis* and the Hg-tolerant strain LBA119, have also been shown to remove more than 80–95% of dissolved Hg(II) through adsorption and enzymatic reduction (Mahbub et al., 2017). Environmental surveys further indicate that genera such as *Proteus, Vibrio*, *Alteromonas, Aeromonas*, and members of *Enterobacteriaceae* possess diverse *mer* gene clusters, enabling effective Hg detoxification in aquatic and terrestrial ecosystems (Quintero et al., 2024).

Although Hg-resistant bacteria have been reported from various contaminated environments, most previous studies have focused mainly on isolate screening and Hg removal efficiency. More comprehensive studies combining bacterial identification, physicochemical analyses, and metabolomic profiling are still limited, especially for indigenous bacteria from Indonesian artisanal and ASGM sites. Therefore, this study investigated an indigenous *Stutzerimonas stutzeri* 08TBb isolate from Hg-contaminated ASGM waste in Jambi Province, Indonesia, using an integrated approach that included tolerance testing, ICP–OES, FTIR, SEM–EDX, and LC-HRMS analyses to better understand its Hg detoxification potential and adaptive responses. This study provides new insight into the application of indigenous bacteria for Hg bioremediation in mining-impacted environments. In addition, the combined use of structural and metabolomic analyses offers a broader understanding of bacterial detoxification mechanisms, which may support the future development of efficient and environmentally friendly remediation strategies.

This study aimed to (1) isolate and screen Hg-tolerant indigenous bacteria from Hg-contaminated gold mining waste; (2) characterize the most effective isolate through morphological, biochemical, and molecular analyses based on the 16S rRNA gene; (3) assess its Hg(II)

removal potential through Hg reduction assays using ICP–OES, Fourier transform infrared spectroscopy (FTIR), and scanning electron microscopy; and (4) identify metabolic compounds associated with Hg detoxification using liquid chromatography–high-resolution mass spectrometry (LC–HRMS). These findings are expected to contribute to the development of an efficient, low-cost, and environmentally friendly bioremediation strategy for Hg-contaminated mining sites, thereby supporting pollution mitigation efforts and sustainable environmental management in ASGM regions.

Materials and methods

1) Collection of samples

Sampling activities were carried out at three artisanal gold-mining sites in Jambi Province, Indonesia, namely, Muara Jernih, Lubuk Gaung, and Bukit Bangkul, which are located within Merangin Regency (Figure 1). These locations were selected because of the continuous use of Hg in the amalgamation process and the direct release of mining effluents into nearby terrestrial and aquatic environments. At each location, triplicate samples of both sediment and water samples were collected. Approximately 250 g of sediment was collected from Hg-contaminated mining areas using sterilized stainless-steel scoops and stored in acid-washed polyethylene bags. Water samples (± 500 mL) were collected directly from mining effluent channels using precleaned high-density polyethylene (HDPE) bottles.

2) Isolation and screening of indigenous bacteria resistant to Hg

A 10-gram sample of sludge was taken and then suspended in 90 mL of sterile distilled water. Moreover, a 1 mL water sample was taken and transferred into 9 mL of sterile distilled water. Next, serial dilution was carried out up to a dilution of 10^{-6}. Each dilution was 0.1 mL and inoculated into nutrient agar (NA) medium containing 20 mg L^{-1} Hg ($HgCl_2$) (Yao et al., 2023). The plate was incubated at 37 °C for 48 hours. The bacterial growth on the media was observed for morphology, and the bacteria were then purified by inoculating bacterial isolates on NA media with the streak method for preservation, after which the bacteria were stored at 4 °C.

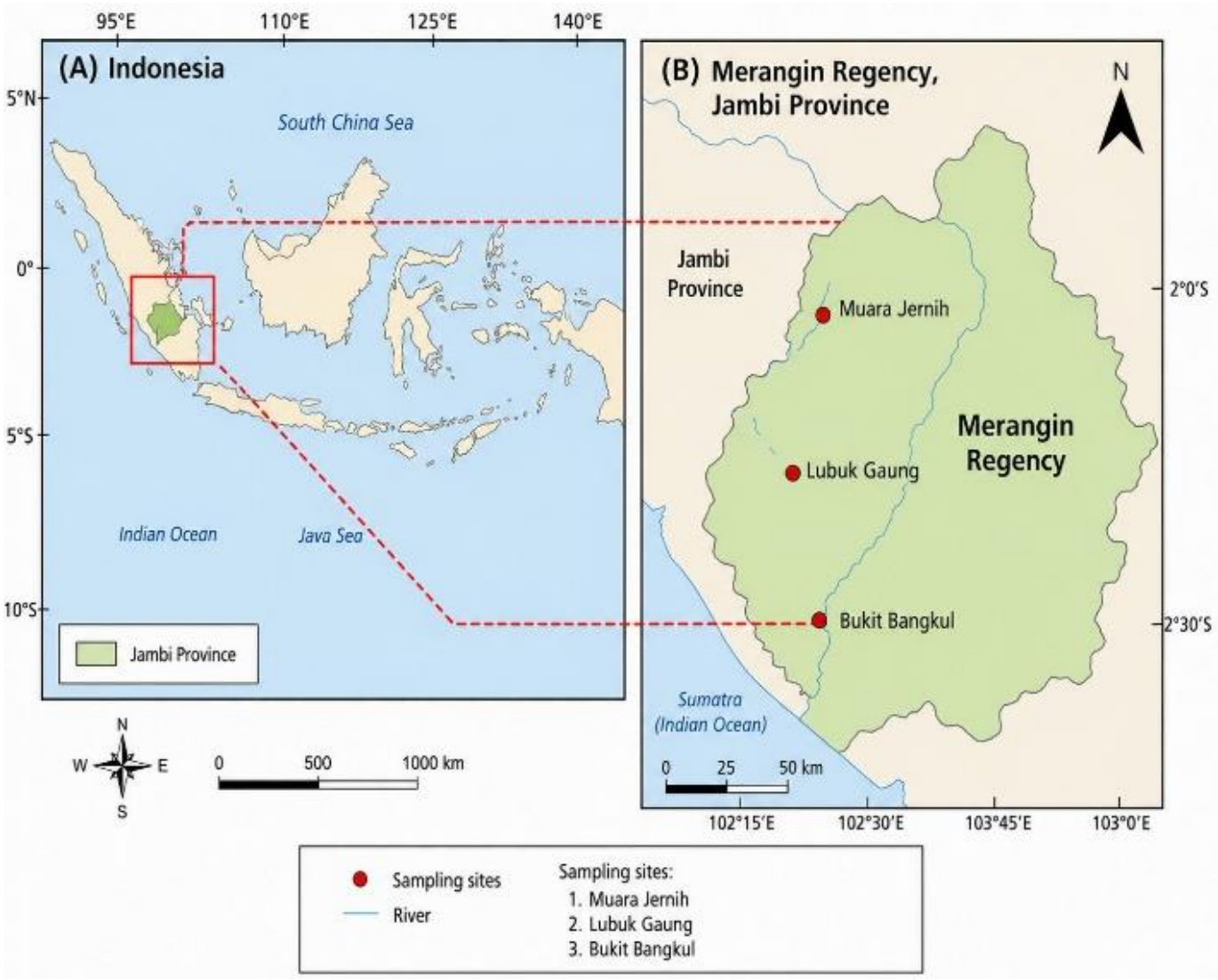

Figure 1 Sampling locations of Hg-contaminated ASGM sites in Jambi Province, Indonesia.

Bacterial isolates that exhibited growth were subsequently subjected to further screening. All the isolates were first subcultured in nutrient broth (NB) for 24 hours and then inoculated into NA media. The resistance of each bacterial isolate to Hg was evaluated by supplementation with $HgCl_2$ at concentrations of 0, 5, 10, 15, 25, 50, 75, and 100 mg L^{-1} using the agar disk diffusion method (Harmoko, 2025). Blank disks were immersed in each $HgCl_2$ concentration for 15 minutes and then placed in NA media that had been inoculated with bacteria and incubated for 24–48 hours. The inhibition zones that developed around the blank disks were used to determine whether the isolates were resistant or sensitive to $HgCl_2$. The diameter of each inhibition zone was measured using a digital caliper according to the criteria shown in Figure 2.

3) Analysis of the Hg resistance levels of bacterial strains

The tolerance of the bacterial strains to Hg was assessed by cultivating them under optimal growth conditions in LB liquid medium supplemented with 0, 25, 50, 75, 100, 150, 200, 250, 400, and 500 mg L^{-1} $HgCl_2$. The media were sterilized at 121 °C for 30 minutes and subsequently inoculated with 2% fresh bacterial culture before being incubated with shaking for 120 hours. To evaluate the Hg tolerance (MTC) of Hg for each strain, the optical density at 600 nm (OD_{600}) was monitored at predetermined time intervals throughout the 120-hour incubation period. The OD measurements were taken regularly using a UV spectrophotometer to characterize the growth response of the strains when they were exposed to Hg stress.

4) Bacterial identification based on morphological, biochemical, and molecular characteristics

The bacterial isolate that exhibited the greatest resistance and tolerance to elevated Hg concentrations was selected for morphological, biochemical, and molecular identification. Morphological characterization was conducted both macroscopically and microscopically. Macroscopic observations included edge, size, surface, color, and elevation, while microscopic observations included shape and gram staining. Biochemical characterization of the bacteria included sugar fermentation tests (glucose, lactose, maltose, mannitol, sucrose, dulcitol, galactose, arabinose, xylose, rhamnose, sorbitol, raffinose, salicin, trehalose, inositol, cellobiose, and aescullin), catalase, oxidase, glucose gas, indole formation, TSIA, citrate, urea, methyl red test (MR test), and Voges–Proskauer test (VP test).

Molecular characterization of the bacterial isolate was performed using 16S rRNA gene sequencing. Genomic DNA was extracted from the selected isolate using the ZymoBIOMICS DNA Miniprep kit. KOD One PCR Master Mix reagents were used for PCR. The universal primers used for amplification were 27F (5'-GAGTTTGATCMTGGCTCAG-3') and 1492R (5'-ACGGYTACCTTGTTACGACTT-3) (Rodiansyah et al., 2021). The PCRs for 40 cycles were performed as follows: predenaturation at 95 °C for 30 s, denaturation at 95 °C for 30 s, annealing at 51 °C for 30 s, extension at 72 °C for 1 min 30 s and postextension at 72 °C for 5 min.

The PCR products were analyzed by electrophoresis using 1% agarose gels prestained with Florosafe DNA Staining, and the DNA bands were subsequently observed under ultraviolet illumination. Following gel verification, the amplicons were subjected to sequencing. The obtained sequences were matched against the GenBank database of the National Center for Biotechnology Information (NCBI) to determine the taxonomic identity of the isolate. A phylogenetic tree was then generated using the neighbor-joining algorithm (distance-based method) implemented in MEGA X software.

5) Assay for Hg reduction by bacterial strains

The bacterial isolate exhibiting the highest level of Hg resistance was subjected to a Hg-reduction assay to evaluate changes in Hg concentration before and after incubation with the organism. First, five inoculation loops of the bacterial culture were transferred into LB broth supplemented with 250 mg L^{-1} $HgCl_2$ and incubated for five days at room temperature with shaking at 120 rpm. At 24-hour intervals, aliquots of the culture were collected and centrifuged at 7,000 rpm for 15 minutes, after which the supernatant was analyzed using ICP to determine the extent of Hg reduction.

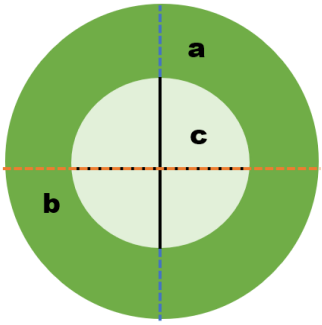

$$Inhibition\ zone = \frac{(a-c)+(b-c)}{2}$$

a = diameter vertical
b = diameter horizontal
c = diameter disk

Figure 2. Schematic illustration of inhibition zone diameter measurement in the agar disc diffusion assay.

Mercury determination was performed using inductively coupled plasma–optical emission spectrometry (ICP–OES) following a wet digestion (microwave-assisted) procedure. Briefly, an accurately weighed or pipetted portion of the sample was placed into a digestion vessel, treated with concentrated nitric acid (HNO_3), and then allowed to predigest for 15 minutes. The vessel was sealed and subjected to microwave digestion until complete mineralization was achieved. After cooling, the digest was quantitatively transferred into a 50 mL volumetric flask, spiked with yttrium as an internal standard, diluted to volume with ultrapure water, homogenized, and filtered. The Hg concentration was subsequently measured by ICP–OES at the selected analytical wavelength using an external calibration curve constructed from at least six mixed standard solutions, and the results were calculated on the basis of the linear regression equation of the calibration curve.

6) Fourier transform infrared (FTIR) analysis

To examine the response mechanism of bacteria under Hg-induced stress, FTIR spectroscopy was employed to characterize alterations in bacterial functional groups before and after exposure to $HgCl_2$. The strain was cultured in LB medium with and without Hg at a concentration of 10 mg L^{-1} for 36 hours. This concentration was selected because it was sufficient to induce measurable Hg stress while maintaining active bacterial growth for subsequent analyses. Following incubation, the cells were harvested by centrifugation at 8,000 rpm for 10 minutes, the supernatant was removed, and the biomass was washed three times with a phosphate buffer solution. The bacterial pellets were subsequently freeze-dried under vacuum. The dried material was finely ground and mixed with potassium bromide (KBr) in an agate mortar at a ratio of 1:100 (biomass:KBr), compressed into thin pellets using a hydraulic press, and analyzed using an FTIR spectrometer over the wavelength range of 4,000–400 cm^{-1}.

7) Scanning electron microscopy (SEM) analysis

Scanning electron microscopy coupled with energy-dispersive X-ray analysis (SEM–EDAX) was utilized to evaluate metal adsorption on the bacterial biomass and to observe any resulting alterations in cell morphology. Biomass samples, both untreated and exposed to 10 mg L^{-1} $HgCl_2$, were rinsed with double-distilled water, spread onto glass slides, and allowed to air-dry.

8) LC-HRMS metabolomic analysis

Untargeted metabolomic analysis of the bacterial isolate was conducted using a Thermo ScientificTM VanquishTM Horizon UHPLC system coupled to an Orbitrap Exploris 240 high-resolution mass spectrometer. Bacterial cultures (1 mL) were centrifuged at 12,000 ×g for 10 min at 4 °C, and the resulting pellet was extracted with cold methanol/acetonitrile/water (2:2:1, v/v/v). The mixture was vortexed, sonicated on ice for 30 min, incubated at −20 °C for protein precipitation, and centrifuged at 14,000 ×g for 20 min. The supernatant was vacuum-dried, reconstituted in 50% acetonitrile, filtered through a 0.20 µm nylon filter, and transferred to LC vials (Kusuma et al., 2025; Windarsih et al., 2022).

Chromatographic separation was performed on an Accucore C18 column (100 mm × 2.1 mm, 2.6 µm) at 40 °C using water (0.1% formic acid) and acetonitrile (0.1% formic acid) as the mobile phases at a flow rate of 0.3 mL min^{-1} with a 25-min gradient program. Mass spectrometric data were acquired in full MS and data-dependent MS modes with polarity switching over a m/z range of 70–800. Metabolite features were processed and annotated using Compound Discoverer software with spectral matching against mzCloud and ChemSpider-based metabolite databases (Kusuma et al., 2025; Windarsih et al., 2022).

Results and discussion

1) Isolation and screening of indigenous bacteria resistant to Hg

A total of 51 bacterial isolates were recovered from Hg-contaminated gold mining waste. These isolates were subsequently screening using a disk diffusion assay with $HgCl_2$ concentrations of 0, 5, 10, 15, 25, 50, 75, and 100 mg L^{-1}. The five bacterial isolates that exhibited the smallest inhibition zones across increasing $HgCl_2$ concentrations were selected as Hg-resistant candidates (Table 1). The isolates showed varying inhibition zone diameters, indicating different levels of Hg tolerance. Several isolates produced larger inhibition zones as the $HgCl_2$ concentration increased, reflecting greater sensitivity to Hg exposure. Five isolates (11TMj, 08TBb, 06ALg, 25ABb, and 28TMj) consistently showed the smallest inhibition zones or no visible inhibition at certain Hg concentrations, suggesting stronger resistance to Hg stress (Table 1). Isolates 11TMj and 28TMj were obtained from soil samples collected at Muara Jernih, isolate 06ALg from water samples at Lubuk Gaung, and isolates 25ABb and 08TBb from water and soil samples collected at Bukit Bangkul, respectively. These findings indicate that Hg -resistant bacteria were present in both soil and water matrices across the contaminated mining sites.

Statistical analysis confirmed significant differences in inhibition zone diameter among bacterial isolates at all tested Hg concentrations (one-way ANOVA, $p < 0.001$). Isolate 08TBb consistently exhibited the smallest inhibition zones, with no detectable growth inhibition up to 25 mg L^{-1} $HgCl_2$ and only minimal inhibition at higher concentrations. These findings indicated that isolate 08TBb possessed superior Hg tolerance compared

with the other indigenous isolates and justified its selection for subsequent MTC determination and detailed characterization. Among these candidates, isolate 08TBb was selected for further study because it showed no detectable inhibition zone up to 25 mg L^{-1} $HgCl_2$ and maintained relatively low inhibition zones at higher concentrations, including a zone smaller than that of isolate 11TMj at 100 mg L^{-1}. This overall resistance profile indicated that isolate 08TBb was the most promising candidate for subsequent MTC and characterization analyses.

The results of the disk diffusion assay clearly revealed differences in Hg tolerance among the bacterial isolates. The selection of isolates producing the smallest or no inhibition zones is based on the principle that reduced growth inhibition reflects an enhanced ability to withstand Hg toxicity (Andrews, 2001). Mercury resistance in bacteria is commonly associated with detoxification mechanisms involving Hg transport proteins such as MerT and MerP, the enzymatic reduction of Hg^{2+} to elemental Hg (Hg^0) by mercuric reductase (MerA), and the degradation of organomercurial compounds by MerB (Freedman et al., 2012). Isolates exhibiting minimal inhibition zones are likely capable of mitigating Hg-induced cellular damage through active detoxification pathways (Boyd and Barkay, 2012).

The absence of inhibition zones in isolates 11TMj, 08TBb, and 28TMj suggests that these bacteria can maintain cellular integrity and metabolic activity under Hg stress. Similar findings have been reported in Hg-resistant bacteria isolated from mining-impacted environments, where resistance is often linked to long-term environmental exposure and selection pressure (Dash and Das, 2012). Furthermore, isolate 08TBb demonstrated no visible inhibition at $HgCl_2$ concentrations up to 50 mg L^{-1}, indicating a strong adaptive response that may involve both extracellular Hg binding and intracellular reduction processes (Barkay et al., 2003). Overall, the screening results support the use of the inhibition zone diameter as an effective preliminary indicator for selecting Hg-resistant bacteria. The five selected isolates represent promising candidates for subsequent studies focusing on the growth kinetics, Hg degradation efficiency, and molecular characterization of resistance genes.

The Hg tolerance (MTC) of selected bacterial isolates was determined on the basis of optical density measurements at 600 nm (OD_{600}) (Figure 3). All the tested isolates (Isolates 06ALg, 08TBb, 25ABb, 11TMj, and 28TMj) exhibited sustained growth across the entire range of Hg concentrations tested, from 25 to 500 mg L^{-1}. Even at the highest concentration (500 mg L^{-1}), the OD_{600}values remained significantly greater than those of the negative control, indicating active bacterial growth. None of the isolates showed complete growth inhibition within the tested concentration range. Therefore, the results were more appropriately interpreted as maximum tolerable concentration (MTC) values greater than 500 ppm rather than minimum inhibitory concentration (MIC). These high MTC values indicated strong Hg tolerance and reflected the adaptation of indigenous bacteria from Hg-contaminated mining waste. Bacterial tolerance to Hg is typically associated with several protective mechanisms, including surface biosorption, intracellular sequestration, active efflux, antioxidant defense, and the enzymatic transformation of toxic Hg species into less reactive forms. These responses help reduce Hg^{2+} toxicity and maintain cellular activity under metal stress.

The sustained OD_{600} values observed in this study indicated that the tested isolates were able to maintain metabolic activity and cellular integrity despite increasing Hg concentrations. This growth pattern may be associated with adaptive mechanisms such as biosorption, transport regulation, oxidative stress defense, and reductive detoxification processes previously described in Hg-resistant bacteria. Previous studies reported that *Pseudomonas stutzeri* was able to grow and survive in media containing $HgCl_2$ and exhibited an active Hg detoxification capacity (Purkan et al., 2016; Zheng et al., 2018). Moreover, previous studies reported that *Stenotrophomonas* sp. isolated from estuarine sediments maintained metabolic activity during Hg exposure and reduced Hg levels by up to 86.9% (Quintero et al., 2024).

Table 1 Screening of indigenous bacterial isolates from Hg-contaminated mining waste on the basis of inhibition zone diameter (mm) under increasing $HgCl_2$ concentrations (0–100 $mg\ L^{-1}$)

No.	Isolate code	Clear zone diameter (mm)							
		0 mg L^{-1}	5 mg L^{-1}	10 mg L^{-1}	15 mg L^{-1}	25 mg L^{-1}	50 mg L^{-1}	75 mg L^{-1}	100 mg L^{-1}
1	11TMj	ND^{e}	ND^{e}	0.2±0.1^{d}	0.3±0.1^{d}	0.5±0.1^{d}	1.5±0.1^{d}	1.9±0.1^{c}	2.7±0.1^{c}
2	28TMj	ND^{e}	ND^{e}	1.4±0.1^{c}	1.7±0.1^{c}	1.7±0.1^{c}	2.1±0.1^{c}	2.3±0.1^{c}	2.6±0.1^{c}
3	06ALg	ND^{e}	ND^{e}	3.6±0.1^{a}	3.6±0.1^{b}	6.1±0.1^{a}	6.3±0.1^{b}	6.5±0.1^{b}	7.1±0.1^{b}
4	25ABb	ND^{e}	ND^{e}	ND^{e}	5.4±0.1^{a}	5.5±0.1^{b}	6.7±0.1^{a}	7.2±0.1^{a}	8.2±0.1^{a}
5	08TBb	ND^{e}	ND^{e}	ND^{e}	ND^{e}	ND^{e}	1.7±0.1^{d}	1.9±0.1^{c}	2.3±0.1^{c}

Notes: TMj (soil sample from Muara Jernih); ALg (water sample from Lubuk Gaung); Abb (water sample from Bukit Bangkul); TBb (soil sample from Bukit Bangkul). The values are presented as the mean ± SD (n = 3). Different superscript letters within the same column indicate significant differences among isolates according to one-way ANOVA followed by Tukey's multiple comparison test ($p < 0.05$). ND = no detectable inhibition zone.

In the present study, isolate 08TBb was able to grow at Hg concentrations up to 500 ppm, indicating a substantially higher tolerance level than that reported for several previously described environmental strains. Isolate 08TBb demonstrated the most consistent growth profile across increasing Hg concentrations, suggesting superior physiological adaptation and detoxification capacity. Consequently, this isolate was selected for further characterization, including morphological observation, biochemical profiling, and molecular identification, to elucidate the genetic and functional basis of its Hg resistance.

2) Bacterial identification based on morphological, biochemical, and molecular characteristics

The morphological characteristics of isolate 08TBb are summarized in Table 2. The isolate formed beige-colored colonies on nutrient agar with a diameter of approximately 1–3 mm (Figure 4-A), an irregular colony shape, undulate margins, and a convex elevation, indicating active surface growth and heterogeneous colony development under laboratory conditions (Cappuccino and Sherman, 2014). Such colony morphology is common in gram-negative bacteria isolated from metal-contaminated environments, where phenotypic plasticity supports survival under chemical stress (Haferburg and Kothe, 2007).

Microscopic observation revealed that isolate 08TBb consisted of rod-shaped (Bacillus) cells and exhibited a gram-negative staining reaction (Figure 4-B) (Cappuccino and Sherman, 2014). The gram-negative cell envelope, characterized by a thin peptidoglycan layer and an outer membrane enriched with lipopolysaccharides, plays a critical role in heavy metal tolerance by providing abundant negatively charged functional groups capable of binding metal ions (Beveridge, 1989). Similar morphological traits have been widely reported for members of the genus *Stutzerimonas*, particularly strains isolated from polluted soils, sediments, and aquatic environments (Lalucat et al., 2006).

The biochemical profile of isolate 08TBb demonstrated broad metabolic versatility (Table 2). Positive fermentation reactions were observed for glucose, lactose, maltose, galactose, xylose, salicin, cellobiose, and aesculin, indicating the ability of the isolate to utilize diverse carbohydrate substrates as energy sources (Cappuccino and Sherman, 2014). Such metabolic flexibility is considered a key adaptive advantage for bacteria inhabiting Hg-contaminated gold mining areas, where nutrient availability is often heterogeneous and unstable (Gadd, 2011).

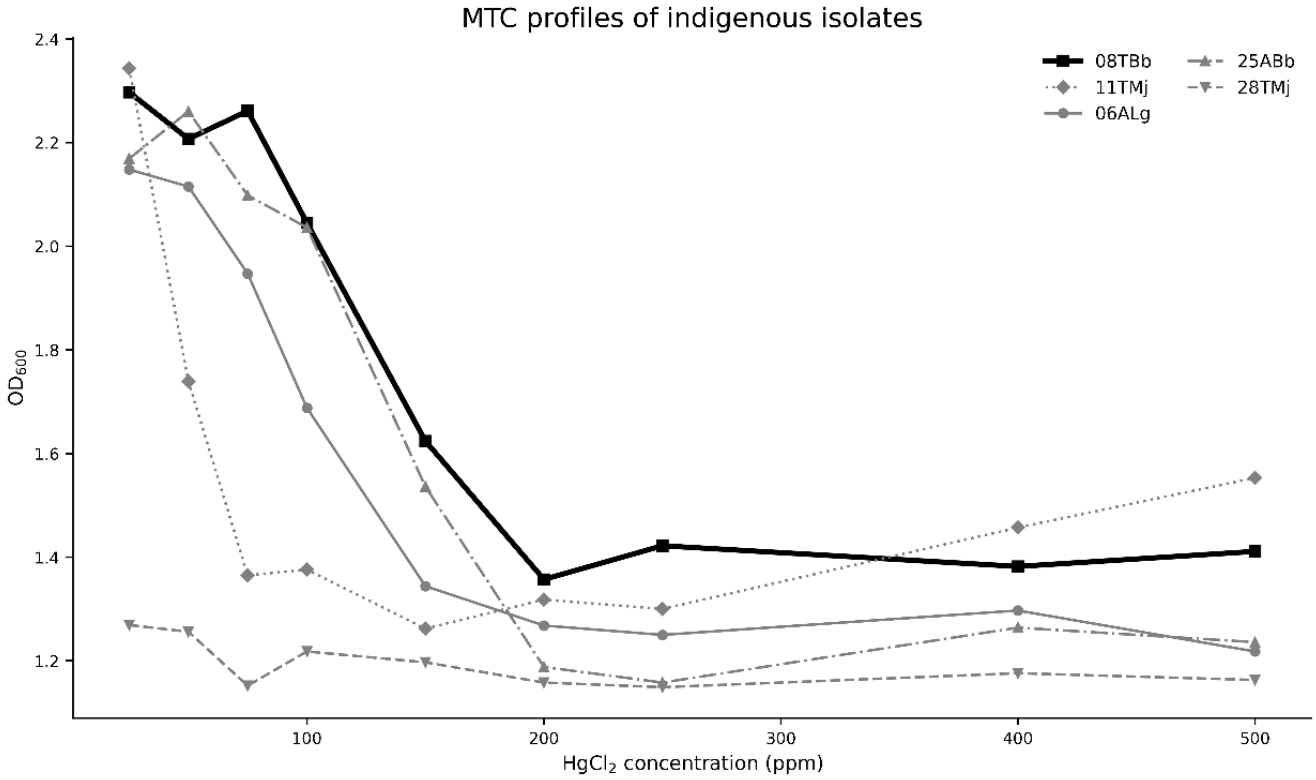

Figure 3 Maximum tolerable concentration (MTC) profiles of indigenous bacterial isolates (08TBb, 11TMj, 06ALg, 25ABb, and 28TMj) cultivated in LB medium supplemented with increasing concentrations of $HgCl_2$ (25–500 ppm).

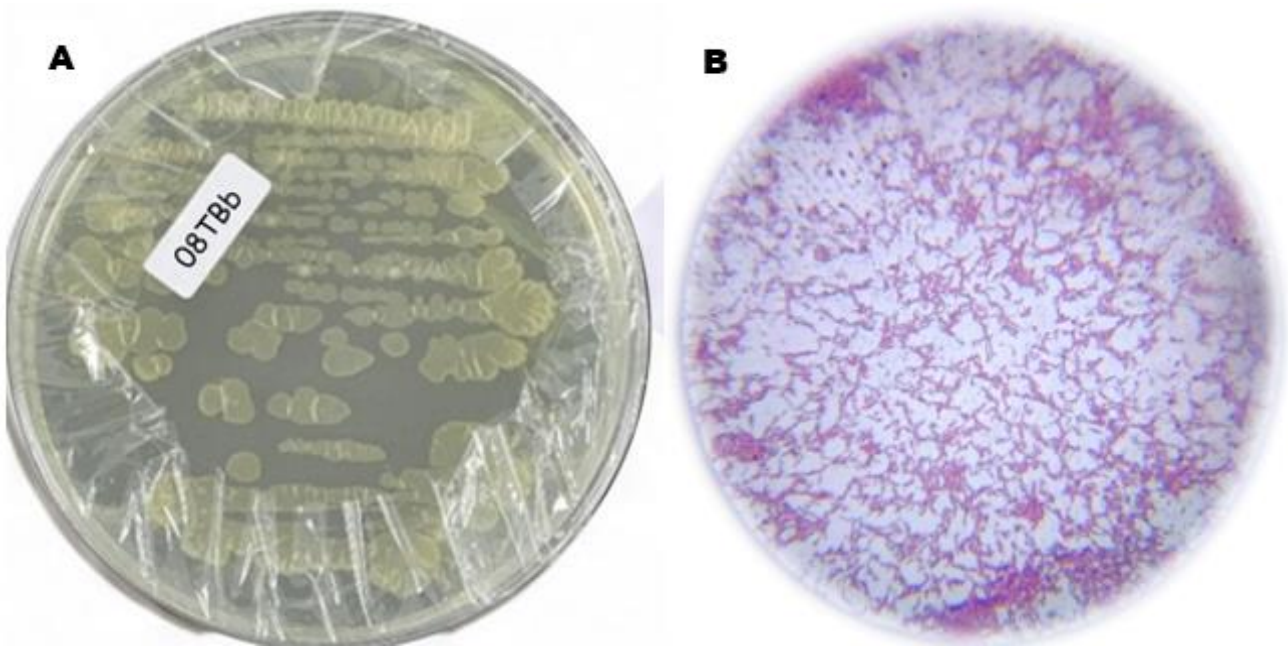

Figure 4 Morphological and microscopic characteristics of isolate 08TBb. (A) Colony morphology of isolate 08TBb grown on nutrient agar medium and (B) Microscopic observation after gram staining.

Table 2 Morphological and biochemical characteristics of *Stutzerimonas stutzeri* 08TBb isolated from Hg-contaminated gold mining waste

Identification test	Results	Identification test	Results
Morphology		**Biochemical**	
- Color of colony at NA	Beige	Glucose fermentation	+
- Colony diameter (mm)	1-3	Lactose fermentation	+
- Colony shape	Irregular	Maltose fermentation	+
- Colony margin	Undulate	Mannitol fermentation	-
- Colony elevation	Convex	Sucrose fermentation	-
- Cell shape	Bacil	Dulcitol fermentation	d
- Gram Staining	Negative	Galactose fermentation	+
Biochemical		Arabinose fermentation	d
- Indol	M/-	Xylose fermentation	+
- TSIA	K/K, H_2S−, Gas−	Rhamnose fermentation	-
- Citrate	+	Sorbitol fermentation	-
- Urea	+	Raffinose fermentation	d
- MR	-	Salicin fermentation	+
- VP	d	Trehalose fermentation	-
- Catalase	+	Inositol fermentation	-
- Oxidase	d	Cellobiose fermentation	+
- Gas glucose	-	Aescullin fermentation	+

Notes: (+) positive reaction; (-) negative reaction; d (delayed reaction/weak reaction); M (motile); K/K (alkaline slant); H_2S (no hydrogen sulfide production); Gas (no gas production); NA (nutrient agar); MR (methyl red); VP (voges-Proskauer); TSIA (triple-sugar iron agar).

The isolate also promoted citrate utilization, urease activity, and catalase production (Cappuccino and Sherman, 2014). Citrate utilization reflects the capacity to exploit alternative carbon sources, whereas urease activity contributes to nitrogen metabolism and local pH regulation (Madigan et al., 2019). Catalase activity indicates an efficient oxidative stress defense mechanism, which is particularly important in Hg-exposed environments because of the induction of reactive oxygen species during metal stress (Nies, 1999). Negative or weak reactions for indole production, methyl red, Voges–Proskauer, and several carbohydrate fermentations suggest that isolate 08TBb primarily relies on oxidative rather than fermentative metabolism (Lalucat et al., 2006). The oxidase reaction was weak or delayed, a trait previously reported for *Stutzerimonas stutzeri* strains, and known to vary depending on environmental conditions and physiological state (Cappuccino and Sherman, 2014; Zheng et al., 2018). Overall, the biochemical characteristics of isolate 08TBb closely resemble those described for *Stutzerimonas species*,

particularly *S. stutzeri*, in previous taxonomic and ecological studies (Lalucat et al., 2006).

Molecular identification of isolate 08TBb was conducted through amplification and sequencing of the 16S rRNA gene. Agarose gel electrophoresis results (Figure 5-(A)) revealed a single, clear DNA band at approximately 1,500 bp, corresponding to the expected size of the bacterial 16S rRNA gene, thereby confirming successful and specific PCR amplification (Weisburg et al., 1991). The absence of nonspecific bands indicates high-quality genomic DNA suitable for phylogenetic analysis (Clarridge, 2004).

Phylogenetic reconstruction based on 16S rRNA gene sequences (Figure 5-(B)) revealed that isolate 08TBb clustered within the *Stutzerimonas stutzeri* lineage. Sequence comparison revealed high similarity (≥ 99%) between isolate 08TBb and the reference strains *Stutzerimonas stutzeri* NR_041715.1 and NR_118798.1. In accordance with established bacterial taxonomic thresholds, a 16S rRNA gene sequence similarity of ≥ 98.7–99.0% is considered strong evidence for species-level identification (Beveridge, 1989; Kim et al., 2014). Therefore, the observed similarity clearly supports the assignment of isolate 08TBb to *Stutzerimonas stutzeri*.

The phylogenetic tree topology further demonstrated that isolate 08TBb formed a monophyletic cluster with *Stutzerimonas stutzeri* reference strains, supported by high bootstrap values (>70%), indicating strong statistical confidence in the inferred evolutionary relationships (Felsenstein, 1985). Closely related species such as *Stutzerimonas xanthomarina*, *Stutzerimonas zhaodongensis*, and *Stutzerimonas nitrititolerans* appeared as neighboring but distinct clades, reflecting interspecific divergence within the genus *Stutzerimonas*. The clear separation of isolate 08TBb from Pseudomonas species and the outgroup Escherichia coli further confirms its taxonomic placement and excludes misidentification at the genus level (Clarridge, 2004; Rosselló-Móra and Amann, 2015).

The strong congruence among the morphological, biochemical, and molecular data provides robust evidence for the accurate identification of the isolate 08TBb as *Stutzerimonas stutzeri* (Kim et al., 2014; Lalucat et al., 2006). The gram-negative rod-shaped morphology and colony characteristics observed in this study are consistent with the phenotypic traits commonly reported for *Stutzerimonas stutzeri*. In parallel, the biochemical profile characterized by oxidative metabolism, broad carbohydrate utilization, and catalase positivity aligns well with the metabolic features described for this species (Lalucat et al., 2006).

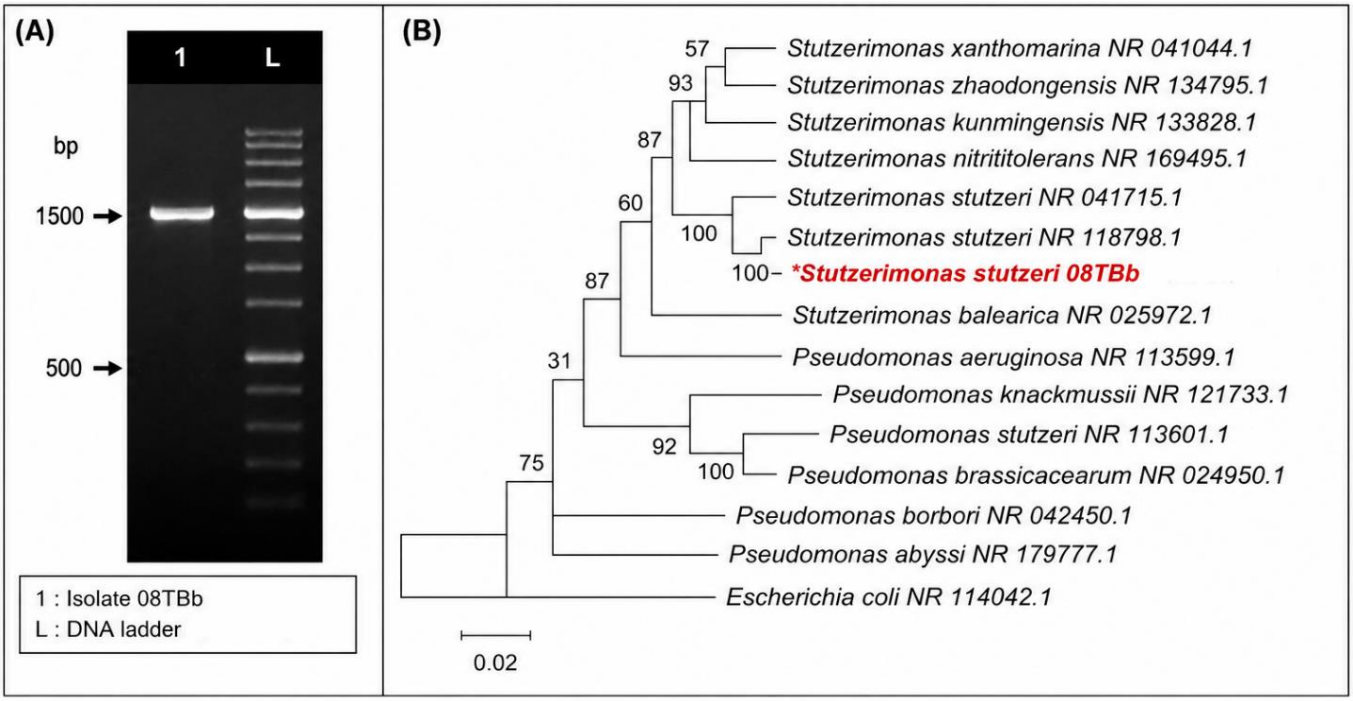

Figure 5 Molecular identification of isolate 08TBb. (A) Agarose gel electrophoresis of the 16S rRNA gene PCR product (~1500 bp). 1: isolate 08TBb; L: DNA ladder. (B) Phylogenetic tree based on 16S rRNA gene sequences showing the phylogenetic position of isolate 08TBb (in red) among closely related species. The numbers at the nodes indicate bootstrap values (%) based on 1000 replications. *Escherichia coli* was used as an outgroup. Scale bar =0.02 substitutions per nucleotide position.

The high 16S rRNA gene sequence similarity (≥99%) further confirms the phenotypic observations and highlights the reliability of a polyphasic taxonomic approach that integrates classical microbiological methods with molecular techniques (Kim et al., 2014; Rosselló-Móra and Amann, 2015). Such an integrated strategy is widely recommended for the accurate classification of environmental bacteria, particularly those isolated from extreme or polluted habitats where phenotypic variability may occur due to adaptive pressure (Pushkar et al., 2019).

Stutzerimonas stutzeri is well known for its ecological versatility and ability to survive in environments contaminated with toxic metals, including Hg (Barkay et al., 2003; Lalucat et al., 2006). Previous studies have demonstrated that Stutzerimonas stutzeri and closely related Hg-resistant bacteria possess multiple Hg detoxification mechanisms, including biosorption on the cell surface, intracellular accumulation, and enzymatic reduction of Hg(II) to the less toxic and volatile Hg (Hg^0) (Boyd and Barkay, 2012; Dash and Das, 2012).

The gram-negative cell wall structure of Stutzerimonas stutzeri, which is enriched with functional groups such as carboxyl, phosphate, and hydroxyl moieties, facilitates the initial binding and immobilization of Hg ions through electrostatic interactions and complexation processes (Beveridge, 1989; Veglio et al., 1997). Furthermore, several *Stutzerimonas stutzeri* strains harbor Hg resistance (*mer*) operons encoding enzymes such as mercuric reductase (MerA), which play a central role in Hg transformation and detoxification (Boyd and Barkay, 2012; Osborn et al., 1997).

The identification of isolate 08TBb as *Stutzerimonas stutzeri*, combined with its isolation from a Hg-contaminated gold mining site and its biochemical traits associated with oxidative stress tolerance, strongly suggests its involvement in Hg degradation processes in situ. These characteristics highlight the ecological importance of the *Stutzerimonas stutzeri* isolate 08TBb and highlight its potential application as a biological agent in Hg bioremediation strategies (Dash and Das, 2012; De et al., 2014).

3) Assay for Hg reduction by bacterial strains

The growth dynamics of *Stutzerimonas stutzeri* 08TBb cultivated in Luria–Bertani (LB) medium supplemented with 250 mg L^{-1} Hg and the corresponding decrease in Hg concentration over a 120-hour incubation period are presented in Figure 6. Statistical analysis confirmed that incubation time significantly affected both bacterial growth and Hg reduction (one-way ANOVA, $p < 0.001$). The OD_{600} values increased progressively from 0 to 120 hours, indicating sustained bacterial proliferation under Hg stress. In contrast, the Hg concentration decreased sharply during the same period, particularly between 24 and 72 hours, suggesting active detoxification during the exponential growth phase. Bacterial growth, expressed as the optical density at 600 nm (OD_{600}), increased progressively throughout the incubation period, indicating that Isolate 08 Tbb was able to survive and proliferate under Hg stress conditions (Barkay et al., 2003). This observation suggests that the isolate possesses an intrinsic Hg resistance mechanism that allows cellular metabolism to proceed despite the presence of a toxic heavy metal (Boyd and Barkay, 2012).

During the initial phase (0–24 hours), bacterial growth is relatively slow, corresponding to the lag phase, in which cells undergo physiological adaptation to Hg-induced stress (Madigan et al., 2019). At this stage, the Hg concentration decreased markedly from its initial value, indicating early Hg removal activity. Such early reduction is typically attributed to rapid adsorption of Hg^{2+} ions onto the bacterial cell surface and cell wall functional groups, including carboxyl, hydroxyl, and phosphate groups (Gadd, 2011). This physicochemical interaction often precedes active intracellular detoxification (Volesky, 2007).

Between 24 and 48 hours, a sharp increase in the OD_{600} was observed, indicating the transition into the exponential growth phase. Concurrently, the Hg concentration substantially decreased, suggesting active biological transformation rather than passive adsorption alone (Dash and Das, 2012). This phase was considered the most important phase for Hg reduction because bacterial metabolic activity and biomass production were at their highest levels. The decrease in the Hg^{2+} concentration during this stage may be associated with several adaptive processes, including enhanced surface biosorption, cellular uptake, and the reductive transformation of Hg ions through the enzymatic detoxification systems described in related strains (Barkay et al., 2003; Dash and Das, 2012). Similar findings were reported in *Pseudomonas stutzeri* and *Cupriavidus metallidurans*, where the highest Hg removal efficiency occurred during the exponential growth phase when cells were metabolically active and capable of maintaining stress-response pathways (Bravo et al., 2020; Zheng et al., 2018). Therefore, the rapid Hg decline observed in isolate 08TBb during 24–48 hours suggested that active growth played an important role in supporting Hg detoxification under elevated metal stress.

From 48 to 72 hours, bacterial growth continued to increase, although at a slower rate, indicating that the late exponential phase approached stationary conditions. The Hg concentration decreased to very low levels during this interval, suggesting that the majority of bioavailable Hg had already been transformed or removed. The strong temporal correlation between increasing bacterial biomass and decreasing Hg

concentration supports the conclusion that Hg removal is predominantly driven by active microbial metabolism rather than abiotic processes (Wang and Greger, 2004).

After 72 hours (96–120 hours), bacterial growth gradually increased, while the Hg concentration remained relatively constant at minimal levels. This pattern is characteristic of the stationary phase, in which nutrient limitation and metabolic byproduct accumulation restrict further growth (Monod, 1949). At this stage, Hg degradation activity likely plateaued because of substrate depletion and reduced metabolic demand (Atlas, 2010). The persistence of bacterial growth under these conditions further confirms the high Hg tolerance of Isolate 08Tbb.

Overall, the results demonstrate a strong coupling between bacterial growth and Hg reduction, with the most effective Hg degradation occurring during the exponential growth phase. These findings are consistent with those of previous studies reporting that Hg bioremediation efficiency is maximized during periods of high cellular activity and enzymatic expression. The ability of Isolate 08Tbb to grow and actively reduce Hg at a concentration of 250 mg L^{-1} highlights its potential application as a bioremediation agent in Hg-contaminated environments.

4) Fourier transform infrared (FTIR) analysis

Fourier transform infrared (FTIR) spectroscopy was applied to elucidate the molecular interactions between Hg and bacterial biomass by comparing the infrared spectra of Hg-containing medium prior to bacterial inoculation (Figure 7-A) and after treatment with *Stutzerimonas stutzeri* 08TBb (Figure 7-B). The comparison reveals significant spectral changes that provide insight into Hg binding, complexation, and transformation processes mediated by the bacterium.

The FTIR spectrum of Hg before bacterial treatment (Figure 7-A) exhibited several characteristic absorption bands associated with inorganic Hg species. The broad absorption in the region of approximately 3,928–3,500 cm^{-1} corresponds to O–H stretching vibrations, indicating the presence of hydrated Hg complexes and hydrogen-bonded water molecules. The peaks observed at approximately 3,582–3,523 cm^{-1} further support the contribution of coordinated hydroxyl groups. The absorption band near 3,149 cm^{-1} is attributed to weakly bound O–H stretching or hydrogen-bonded water molecules associated with Hg^{2+} ions. A prominent band at approximately 1,611 cm^{-1} is assigned to H–O–H bending vibrations, confirming the aqueous nature of the Hg species. Importantly, a distinct absorption band detected at approximately 454 cm^{-1} is characteristic of Hg–Cl stretching vibrations, which is consistent with the presence of Hg in the form of inorganic salts such as $HgCl_2$ in the medium (Nakamoto, 2008; Rytuba, 2003).

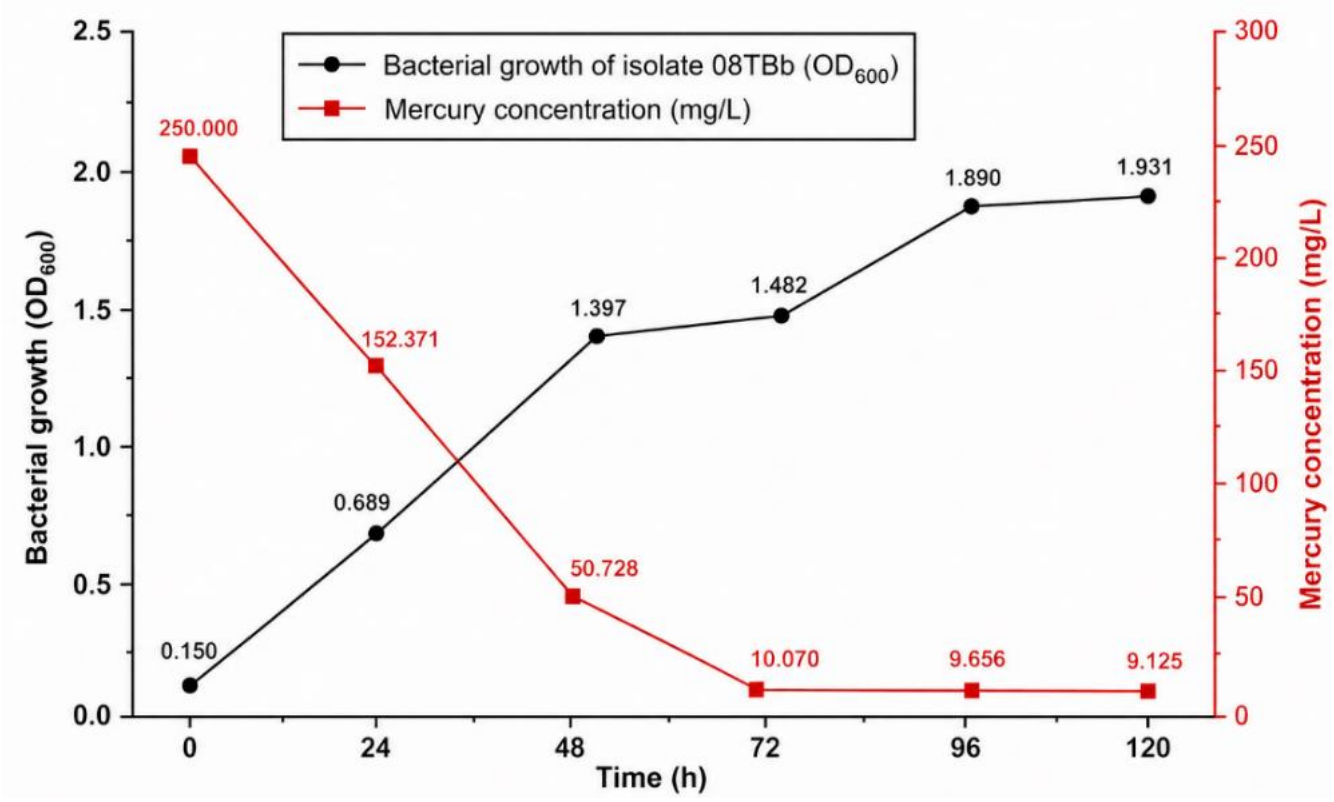

Figure 6 Growth of *Stutzerimonas stutzeri* 08TBb (OD_{600}) in LB medium containing 250 mg L^{-1} $HgCl_2$ and concurrent Hg removal over 120 hours. The values are presented as the mean ± SD (n=3). The bacterial growth increased significantly over time, whereas the Hg concentration decreased significantly (one-way ANOVA, $p < 0.001$).

Following incubation with Stutzerimonas stutzeri (Figure 7-B), pronounced modifications in the FTIR spectrum were observed, indicating strong interactions between Hg and bacterial functional groups. The O–H stretching region (3,600–3,200 cm^{-1}) became broader and less defined, suggesting enhanced hydrogen bonding and the involvement of hydroxyl groups from bacterial cell wall components and extracellular polymeric substances (EPSs). This broadening reflects the formation of Hg–O coordination bonds between the Hg^{2+} ions and the hydroxyl or carboxyl groups present in the polysaccharides and proteins on the bacterial surface (Baldi et al., 2017).

Additionally, clear changes were observed in the region at approximately 2,920–2,850 cm^{-1}, corresponding to the C–H stretching vibrations of aliphatic chains. The altered intensity of these bands after bacterial treatment indicates structural rearrangement of membrane lipids or EPS components induced by Hg binding. Significant modifications were also detected in the amide region, particularly between 1,650 and 1,540 cm^{-1}, which corresponds to amide I (C=O stretching) and amide II (N–H bending) vibrations. The shifting and intensity reduction of these bands suggest the direct involvement of protein functional groups in Hg binding, suggesting that surface proteins and enzymes participate in Hg immobilization (Wang and Chen,2009).

A critical spectral change was observed in the low wavenumber region below 600 cm^{-1}. After bacterial treatment, the intensity of the Hg–Cl stretching band near 454 cm^{-1} markedly decreased or partially disappeared. This attenuation indicates the disruption of Hg–Cl bonds and suggests that Hg was released from its original inorganic chloride form. The loss of this characteristic vibration strongly implies chemical transformation of Hg, whereby Hg^{2+} ions are detached from chloride ligands and subsequently complexed by bacterial functional groups or enzymatically reduced (Upadhyay et al., 2017).

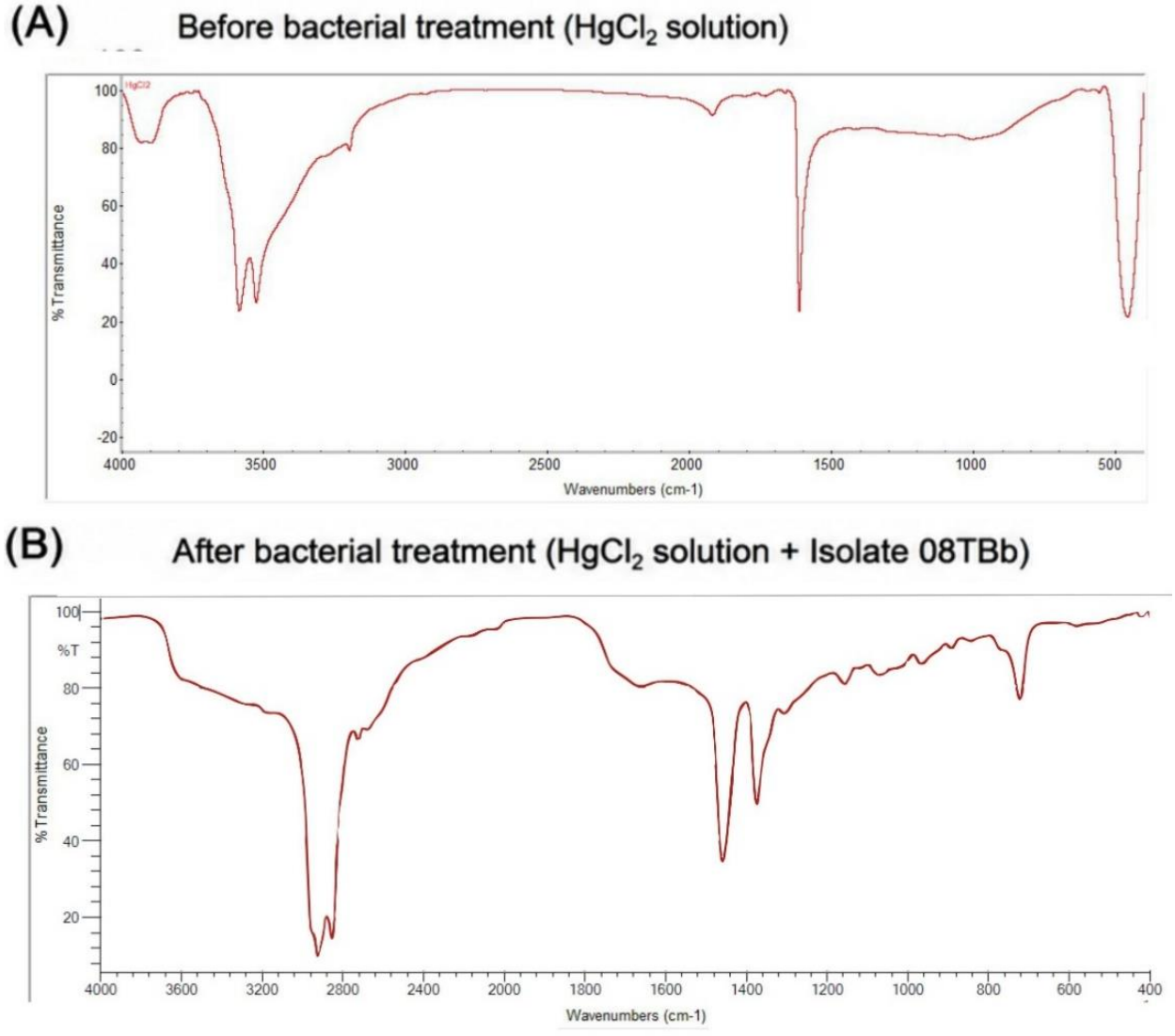

Figure 7 Comparative FTIR spectra of $HgCl_2$ before (A) and after treatment with *Stutzerimonas stutzeri* 08TBb (B), illustrating changes in functional groups associated with microbial mercury binding and transformation.

The observed differences in the FTIR spectra before and after bacterial treatment provide strong evidence that *Stutzerimonas stutzeri* 08TBb mediates Hg removal through a sequential adsorption–degradation mechanism. Initially, Hg^{2+} ions are adsorbed onto the bacterial surface via coordination with hydroxyl, carboxyl, phosphate, and amide groups, as indicated by shifts and broadening in the corresponding FTIR bands. Subsequently, a fraction of the surface-bound Hg undergoes biochemical transformation, likely mediated by Hg resistance enzymes, which reduce toxic Hg(II) to elemental Hg [Hg(0)]. Although Hg(0) is not directly detectable by FTIR because of its volatile nature, the disappearance or weakening of Hg–Cl vibrations provides indirect evidence supporting this transformation process (Barkay et al., 2003).

Similar FTIR-based observations were reported for several Hg-tolerant bacteria, including *Bacillus licheniformis*, *Pseudomonas putida*, and *Sphingopyxis* sp. In those studies, shifts in the absorption bands of hydroxyl, carboxyl, phosphate, and amide groups after Hg exposure were interpreted as evidence of biosorption followed by metal stabilization or transformation processes (Mahbub et al., 2017; Nies, 1999; Upadhyay et al., 2017; Wang and Chen, 2009). Mercury binding by *Bacillus licheniformis* is closely associated with extracellular polymeric substances containing oxygen- and nitrogen-rich functional groups, which promote rapid Hg^{2+} immobilization (Upadhyay et al., 2017). Changes in the FTIR peak of *Sphingopyxis* sp. SE2, particularly in the carboxyl and hydroxyl regions, indicate the involvement of cell-surface ligands during Hg uptake (Mahbub et al., 2017). Bacterial biomass can modify metal speciation through surface complexation, ion exchange, and subsequent detoxification reactions (Wang and Chen, 2009). Similar responses have also been described in *Pseudomonas putida*, where changes in amide and phosphate bands suggested the participation of proteins and membrane-associated groups in heavy metal sequestration (Nies, 1999). Taken together, these previous studies support the interpretation that isolate 08TBb may have applied comparable physicochemical mechanisms for Hg removal.

Overall, FTIR analysis demonstrated that bacterial treatment significantly altered the chemical environment of Hg in the medium. The transition from inorganic Hg–Cl bonds to Hg–biomolecule complexes, followed by enzymatic reduction, highlights the effective role of *Stutzerimonas stutzeri* in Hg adsorption and degradation. These molecular-level findings are consistent with the SEM–EDX and ICP–OES results, collectively confirming the strong bioremediation potential of this bacterium.

5) Scanning electron microscopy (SEM) and energy dispersive X-ray (EDX) analysis

Scanning electron microscopy (SEM) analysis revealed distinct morphological differences between *Stutzerimonas stutzeri* 08TBb cells cultivated in Hg-free medium (Figure 8-A) and those exposed to Hg -containing medium (Figure 8-B). In the absence of Hg, bacterial cells exhibited relatively smooth and uniform surface textures, with compact cell aggregation and no visible particulate deposits on the cell envelope. The surface appeared intact and homogeneous, reflecting normal physiological conditions and balanced cellular metabolism. This morphology is typical of gram-negative bacteria growing under nonstress conditions, where cell wall integrity and membrane organization remain unaltered (Leboffe and Pierce, 2016).

In contrast, *Stutzerimonas stutzeri* 08TBb cells grown in Hg-containing medium (Figure 5-B) displayed pronounced morphological alterations. SEM images revealed markedly roughened and irregular cell surfaces, accompanied by extensive agglomeration and granular deposits covering the bacterial biomass. These surface features indicate a stress-induced adaptive response, in which bacterial cells actively modify their surface architecture to mitigate Hg toxicity. The presence of surface-associated particles strongly suggests the extracellular accumulation of Hg, either adsorbed directly onto the cell wall or entrapped within extracellular polymeric substances (EPSs). Similar surface roughening and particle deposition have been reported in Hg-resistant bacteria exposed to Hg(II), serving as visual indicators of biosorption processes (Upadhyay et al., 2017).

Energy dispersive X-ray (EDX) spectra further supported these SEM observations. Cells grown without Hg (Figure 8-C) were dominated by carbon (C) and oxygen (O), corresponding to organic cellular components such as proteins, lipids, and polysaccharides, with minor contributions from sodium (Na) and chlorine (Cl) originating from residual culture medium salts. Notably, no Hg-related peaks were detected, confirming the absence of Hg accumulation on the bacterial surface under control conditions. This elemental profile indicates that in the absence of heavy metal stress, *Stutzerimonas stutzeri* 08TBb does not exhibit enhanced metal binding behavior or extracellular mineral deposition.

EDX analysis of Hg-exposed cells provided direct evidence supporting this interpretation. In addition to the dominant carbon and oxygen signals, distinct Hg-related peaks were detected in the spectra, confirming the association of Hg with the bacterial biomass. The simultaneous presence of Na and Cl alongside Hg suggests that ion-exchange mechanisms may have occurred, whereby Hg^{2+} ions displaced lighter cations at negatively charged binding sites on the cell surface. This process is consistent with the high affinity of Hg for functional groups containing sulfur, oxygen, and nitrogen atoms, which are abundant in bacterial cell walls and EPS matrices (Wang and Chen, 2009). The combined SEM–EDX results indicate that Hg removal

by *Stutzerimonas stutzeri* 08TBb involves an initial biosorption phase. During this stage, Hg^{2+} ions are rapidly immobilized on the cell surface through electrostatic attraction, complexation, and coordination with functional groups such as carboxyl ($–COO^-$), hydroxyl (–OH), phosphate ($–PO_4^{3-}$), and particularly sulfhydryl (–SH) groups (Aslam et al., 2025; Shamim, 2018). Mercury is classified as a soft Lewis acid and therefore has a strong binding affinity toward sulfur-containing ligands, which explains its preferential association with thiol-rich proteins and EPS components observed as surface deposits in SEM images (Baldi et al., 2017).

Beyond surface adsorption, the morphological changes observed in Hg-exposed cells also imply the occurrence of Hg degradation or transformation processes. The roughened surfaces, particle deposition, and cell aggregation indicated that *Stutzerimonas stutzeri* 08TBb responded actively to Hg stress by modifying its cell envelope and increasing the availability of binding sites for Hg^{2+} ions. Such responses are commonly associated with extracellular sequestration, intracellular accumulation, and stress-induced restructuring of membrane components in metal-tolerant bacteria (Nies, 1999). Although SEM cannot directly visualize enzymatic reduction or volatilization, the extensive surface binding observed likely represents a preliminary step in which Hg is concentrated at the cell interface prior to intracellular uptake and enzymatic detoxification (Boyd and Barkay, 2012).

Comparative SEM–EDX analysis clearly demonstrated that *Stutzerimonas stutzeri* 08TBb employs a dual Hg remediation strategy. Under Hg-free conditions, the bacterium maintains normal cellular morphology and elemental composition. In contrast, exposure to Hg induces significant surface modification, enhanced biosorption, and Hg accumulation on the cell envelope, followed by biochemical transformation mechanisms. This integrated response highlights the strong adaptive capacity of *Stutzerimonas stutzeri* 08TBb and supports its potential application as an effective biological agent for Hg bioremediation in contaminated environments.

6) LC-HRMS metabolomic analysis

Untargeted LC–HRMS metabolomic analysis of *Stutzerimonas stutzeri* 08TBb exposed to Hg revealed a distinct metabolic signature dominated by sulfur-containing compounds, stress-related amino acids and peptides, osmoprotectants, nucleotides, and membrane-associated lipids (Table 3) (Cajka and Fiehn, 2016; Chiaramonte et al., 2018). The detection of these metabolites indicates that Hg exposure induces a coordinated metabolic response involving metal binding, redox regulation, and cellular structural adaptation (Kåhrström, 2014). Such a response is characteristic of Hg-resistant bacteria and provides molecular evidence supporting the bioremediation potential of *Stutzerimonas stutzeri* (Dash and Das, 2012).

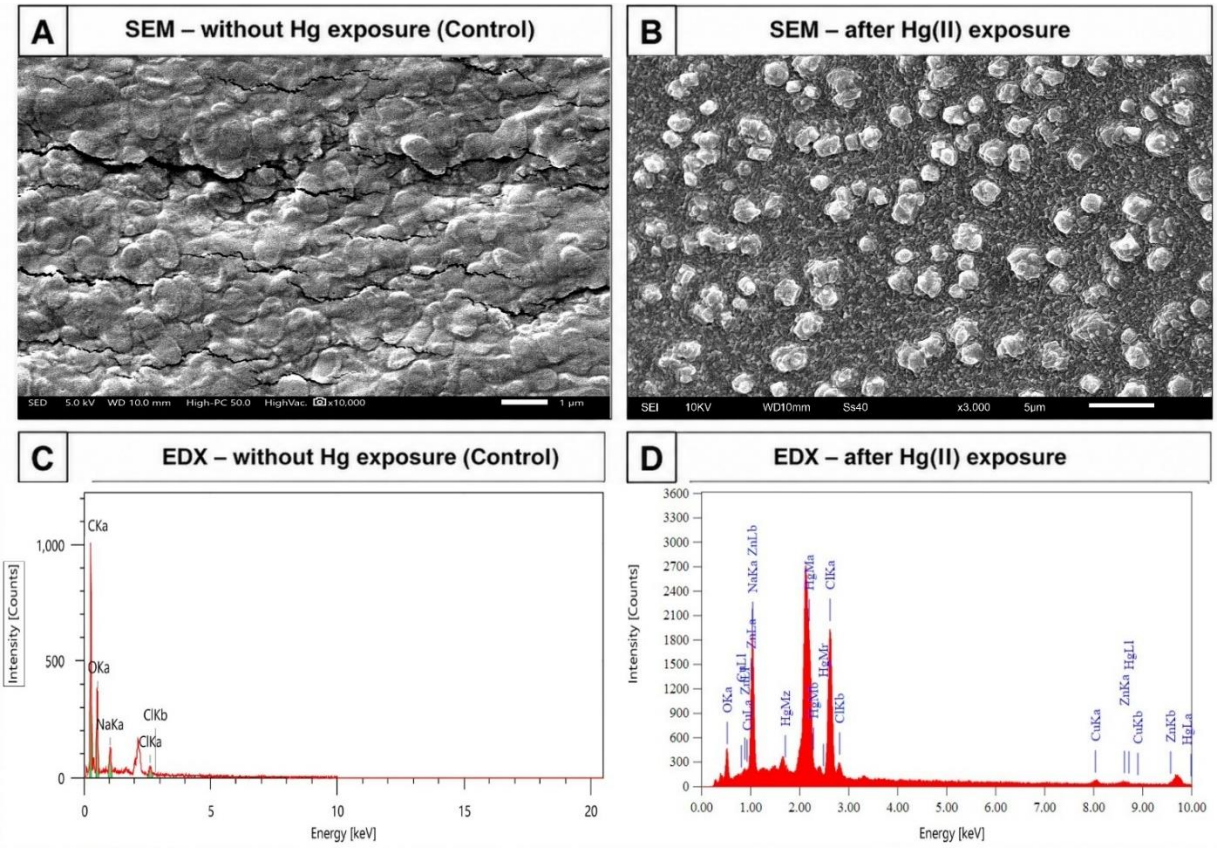

Figure 8 Comparative SEM micrographs and EDX spectra of *Stutzerimonas stutzeri* 08TBb grown without Hg (A, C) and after Hg(II) exposure (B, D).

Table 3 Top 20 discriminant metabolites of *Stutzerimonas stutzeri* 08TBb associated with Hg degradation identified by LC–HRMS

No.	Metabolite	Molecular formula	RT (min)	m/z	Metabolite class	Proposed role in mercury degradation
1	Glutathione (reduced)	$C_{10}H_{17}N_3O_6S$	0.76	308.09	Thiol compound	Direct chelation of Hg^{2+} via –SH groups and intracellular redox buffering (Barkay et al., 2003; Boyd and Barkay, 2012)
2	Glutathione disulfide (GSSG)	$C2_0H_{32}N_6O_{12}S_2$	0.82	613.16	Antioxidant	Indicator of oxidative stress generated during Hg detoxification (Boyd and Barkay, 2012; Gadd, 2011)
3	Cysteine	$C_3H_7NO_2S$	0.61	121.02	Sulfur amino acid	Precursor for thiol-based Hg binding and glutathione biosynthesis (Barkay et al., 2003; Dash and Das, 2012)
4	Methionine	$C_5H_{11}NO_2S$	0.67	149.05	Sulfur amino acid	Protection against Hg-induced oxidative damage and protein stabilization (Gadd, 2011; Hillion and Antelmann, 2015)
5	Lysine	$C_6H_{14}NO_2S_2$	0.65	146.11	Amino acid	Stress-induced protein synthesis and modulation of cell surface charge (Kim et al., 2014)
6	Phenylalanine	$C_9H_{11}NO_2$	0.69	165.08	Amino acid	Supports stress-responsive protein turnover under metal toxicity (Min et al., 2020)
7	Glycyl-leucine	$C_8H_{16}N_2O_3$	0.73	188.12	Dipeptide	Proteostasis and peptide recycling during Hg stress (Min et al., 2020)
8	Leucyl-proline	$C_{11}H_{20}N_2O_3$	0.74	228.15	Dipeptide	Stress signaling and metabolic adaptation to heavy metals (Li et al., 2025)
9	Cyclo(Lys–Pro)	$C_{11}H_{20}N_2O_2$	3.15	212.15	Cyclic dipeptide	Metal-stress signaling and biofilm-associated protection (Li et al., 2025)
10	Mannitol	$C_6H_{14}O_6$	0.88	182.08	Polyol	ROS scavenging and osmoprotection during Hg exposure (Gadd, 2011; Sleator and Hill, 2002)
11	Betaine	$C_5H_{11}NO_2$	0.75	118.09	Osmolyte	Protein stabilization and oxidative stress tolerance (Ali et al., 2020; Sleator and Hill, 2002)
12	Threonic acid	$C_4H_8O_5$	0.72	136.04	Organic acid	Antioxidant-related metabolism during metal stress (Gadd, 2011)
13	AMP	$C_{10}H_{14}N_5O_7P$	0.72	347.06	Nucleotide	Increased ATP demand for Hg detoxification and repair mechanisms (Nies, 2016)
14	GMP	$C_{10}H_{14}N_5O_8P$	0.76	363.06	Nucleotide	Enhanced nucleotide turnover under heavy-metal stress Nies, 2016
15	Nicotinamide	$C_6H_6N_2O$	0.68	122.05	Redox cofactor	Maintenance of NAD^+/NADH balance during Hg reduction [26]
16	Hexadecanamide	$C_{16}H_{33}NO$	15.42	255.26	Fatty amide	Membrane stabilization to limit Hg penetration (Capdevila et al., 2024)
17	Stearamide	$C_{18}H_{37}NO$	16.37	283.29	Fatty amide	Increased membrane rigidity under metal stress (Capdevila et al., 2024)
18	Monoacylglycerol (16:0)	$C_{19}H_{38}O_4$	15.78	330.28	Lipid	Cell membrane remodeling and barrier reinforcement (Capdevila et al., 2024)
19	Phosphatidylcholine fragment	$C_8H_{20}NO_6P$	12.10	257.09	Phospholipid	Surface adsorption of Hg^{2+} and envelope adaptation (Wang and Chen, 2009)
20	Spermidine	$C_7H_{19}N_3$	0.64	145.17	Polyamine	Protection against oxidative and heavy-metal stress (Ayoola et al., 2019)

As shown in Table 3, reduced glutathione was identified as one of the most biologically relevant discriminant metabolites associated with Hg degradation (Schafer and Buettner, 2001). Glutathione is a low-molecular-weight thiol that plays a pivotal role in Hg detoxification through direct chelation of Hg(II) via sulfhydryl (–SH) groups, resulting in the formation of stable Hg–S complexes (Clarkson and Magos, 2006). This mechanism effectively decreases intracellular Hg toxicity and protects essential proteins from thiol oxidation (Ballatori et al., 2009). Glutathione also contributes to maintaining redox balance during heavy-metal stress by neutralizing reactive oxygen species generated during Hg exposure (Clarkson and Magos, 2006; Schafer and Buettner, 2001). Similar findings have been reported in Hg -resistant bacteria and other metal-tolerant microorganisms, where elevated glutathione levels were associated with improved survival and enhanced detoxification capacity under Hg stress. Glutathione is a central component of cellular redox regulation, and the strong affinity of Hg for thiol-containing biomolecules has been emphasized (Clarkson and Magos, 2006; Schafer and Buettner, 2001). *Sphingopyxis* sp. utilized intracellular thiol-based defense systems during Hg remediation (Mahbub et al., 2017). These findings support the interpretation that the glutathione detected in isolate 08TBb played important roles in Hg binding, oxidative stress protection, and overall cellular adaptation during Hg detoxification.

In addition to glutathione, several sulfur- and nitrogen-containing metabolites, including thiourea derivatives and sulfonated compounds (Table 3), were detected. Mercury is classified as a soft Lewis acid and has a strong affinity toward soft base ligands such as sulfur- and nitrogen-containing functional groups. The detection of these metabolites indicates that *Stutzerimonas stutzeri* 08TBb facilitates Hg immobilization not only through enzymatic reduction but also through chemical complexation. This interpretation is consistent with the FTIR results showing alterations in functional groups involved in Hg binding and with the SEM–EDX observations demonstrating Hg accumulation on the bacterial surface.

Amino acids and short peptides, including lysine, phenylalanine, glycyl-leucine, and leucyl-proline, were also prominent among the discriminant metabolites (Table 3). These compounds are typically associated with stress-induced protein turnover and cellular repair mechanisms. Mercury exposure is known to damage proteins by binding to thiol groups and disrupting tertiary structures; therefore, enhanced amino acid and peptide metabolism likely reflects the active synthesis and replacement of damaged proteins (Delaney et al., 2019). Moreover, positively charged amino acids such as lysine may influence the electrostatic properties of the bacterial cell surface, indirectly enhancing Hg absorption at the cell envelope.

Compatible solutes and polyols, such as betaine and mannitol (Table 3), were detected and are widely recognized for their role in osmoprotection and oxidative stress mitigation. Mercury toxicity is often accompanied by the generation of reactive oxygen species (ROS), leading to oxidative damage to lipids, proteins, and nucleic acids. The accumulation of these metabolites suggests that *Stutzerimonas stutzeri* activates protective mechanisms to maintain redox balance and cellular integrity during Hg stress (Kempf and Bremer, 1998).

Nucleotide-related metabolites, including adenosine monophosphate (AMP) and guanosine monophosphate (GMP), were identified among the discriminant features (Table 3), indicating increased nucleotide turnover and energy demand. These metabolic shifts are consistent with elevated ATP requirements for active detoxification processes, including Hg transport, the repair of damaged biomolecules, and the enzymatic reduction of Hg(II). The metabolic investment in energy-related pathways supports the involvement of active Hg resistance systems rather than passive adsorption alone (Andrews, 2001).

Furthermore, lipid-related metabolites such as monoacylglycerols, fatty acid amides, and phosphatidylcholine fragments were detected (Table 3), indicating that membrane remodeling occurred in response to Hg exposure. Mercury is known to disrupt membrane integrity by interacting with membrane proteins and phospholipids. Therefore, increased lipid turnover likely represents an adaptive response to reinforce membrane structure and limit Hg penetration into the cytoplasm. These metabolomic findings are consistent with SEM observations of altered cell surface morphology under Hg stress (Tromas et al., 2020).

Overall, the LC–HRMS metabolomic profile demonstrated that *Stutzerimonas stutzeri* 08TBb employs a multi-faceted Hg degradation strategy. As summarized in Table 3, Hg removal involves (i) surface adsorption and chemical complexation mediated by sulfur- and nitrogen-containing metabolites, (ii) intracellular detoxification through thiol-based chelation and enzymatic reduction, and (iii) metabolic reprogramming to mitigate oxidative stress and maintain membrane integrity. When integrated with the SEM–EDX, FTIR, and ICP–OES results, these findings provide a comprehensive mechanistic framework explaining how *Stutzerimonas stutzeri* 08TBb effectively degrades and detoxifies Hg in contaminated environments.

Conclusions

A total of 51 bacterial isolates were obtained through the isolation and screening of indigenous bacteria from Hg-contaminated gold mining sites. Among these isolates, the most effective strain was comprehensively characterized using morphological, bioche-

mical, and molecular approaches and was identified as *Stutzerimonas stutzeri* 08TBb. The selected isolate demonstrated a strong ability to tolerate high Hg concentrations and actively reduced Hg(II) levels, as quantified by ICP–OES analysis and further supported by FTIR and SEM observations. These analyses revealed that Hg detoxification involved chemical interactions with bacterial functional groups and structural adaptations of the cell surface, indicating efficient adsorption and transformation processes. Furthermore, metabolomic analysis revealed key sulfur-containing and stress-related metabolites associated with Hg detoxification, highlighting the involvement of coordinated metabolic pathways in metal binding, redox regulation, and cellular protection. Overall, these findings indicate that indigenous *Stutzerimonas stutzeri* 08TBb has significant potential as a low-cost and environmentally friendly bioremediation agent for Hg-contaminated mining environments. This study provides valuable scientific insights into microbial Hg detoxification mechanisms and supports the development of sustainable bioremediation strategies to mitigate pollution in artisanal and small-scale gold mining regions.

Acknowledgements

The authors gratefully acknowledge the financial support provided by the Direktorat Riset, Teknologi, dan Pengabdian kepada Masyarakat (DRTPM), Kementerian Pendidikan, Kebudayaan, Riset, dan Teknologi Republik Indonesia, through the 2025 Penelitian Dosen Pemula grant scheme. The authors also sincerely thank the Integrated Laboratory of Universitas Nahdlatul Ulama Pasuruan for supplying the research facilities essential to the completion of this research.

Data availability statement

Information and data used in the study will be disclosed upon request.

Author ORCID

Uun Rohmawati: 0009-0004-5605-5323
Juanita Hibatullah: 0000-0003-4460-7528
Achmad Rodiansyah: 0000-0001-5565-1386
Yunita Messe: 0000-0002-6465-6645
Dwi Nur Aini Fajriah: 0009-0007-9690-8601

Author contributions

Uun Rohmawati: Conceptualization, Methodology, Validation, Investigation, Resources, Data curation, Writing – Original draft, Writing – Review & editing, Supervision, Project administration, Funding acquisition
Juanita Hibatullah: Software, Formal analysis, Investigation, Data curation, Writing – Review & editing, Visualization
Achmad Rodiansyah: Software, Formal analysis, Investigation, Visualization
Yunita Messe: Formal analysis, Investigation, Resources, Project administration
Dwi Nur Aini Fajriah: Formal analysis, Investigation, Resources, Visualization

Conflicts of interest

The authors declare that there are no conflicts of interest in competing financial or personal relationships that could have appeared to influence the work reported in this work.

References

Ali, S., Abbas, Z., Seleiman, M. F., Rizwan, M., Yavaş, İ., Alhammad, B. A., Shami, A., Hasanuzzaman, M., & Kalderis, D. (2020). Glycine betaine accumulation, significance and interests for heavy metal tolerance in plants. *Plants*, *9*(7), 896.

Andrews, J. M. (2001). Determination of minimum inhibitory concentrations. *Journal of Antimicrobial Chemotherapy*, *48*(Suppl. S1), 5–16.

Aslam, A., Kanwal, F., Javied,S., Nisar, N., & Torriero, A. A. J. (2025). Microbial biosorption: A sustainable approach for metal removal and environmental remediation. *International Journal of Environmental Science and Technology*, *22*, 13245–13276.

Atlas, R. M. (2010). *Handbook of microbiological media* (4th ed.) Boca Raton: CRC Press.

Ayoola, M. B., Shack, L. A., Nakamya, M. F., Thornton, J. A., Swiatlo, E., & Nanduri, B. (2019). Polyamine synthesis effects capsule expression by reduction of precursors in *streptococcus pneumoniae*. *Frontiers in Microbiology*, *10*, 1996.

Baldi, F., Gallo, M., Daniele, S., Battistel, D., Faleri, C., Kodre A, & Arcon, I. (2017). An extracellular polymeric substance quickly chelates mercury(II) with N-heterocyclic groups. *Chemosphere*, *176*, 296–304.

Ballatori, N., Krance, S. M., Notenboom, S., Shi, S., Tieu, K., & Hammond, C. L. (2009). Glutathione dysregulation and the etiology and progression of human diseases. *Biological Chemistry*, *390*, 191–214.

Barkay, T., Miller, S. M., & Summers, A. O. (2003). Bacterial mercury resistance from atoms to ecosystems. *FEMS Microbiology Reviews*, *27*, 355–384.

Beveridge, T. J. (1989). Role of cellular design in bacterial metal accumulation and mineralization. *Annual Review Microbiology*, *43*, 147–171.

Boyd, E. S., & Barkay, T. (2012). The mercury resistance operon: From an origin in a geothermal environment to an efficient detoxification machine. *Frontier in Microbiology*, *3*, 349.

Bravo, G., Vega-Celedón, P., Gentina, J. C., & Seeger, M. (2020). Effects of mercury II on *Cupriavidus metallidurans* strain MSR33 during mercury biore-

mediation under aerobic and anaerobic conditions. *Processes*, *8*, 893.

Cajka, T., & Fiehn, O. (2016). Toward merging untargeted and targeted methods in mass spectrometry-based metabolomics and lipidomics. *Analytical Chemistry*, *88*, 524–545.

Capdevila, D. A., Rondón, J. J., Edmonds, K. A., Rocchio, J. S., Dujovne, M. V., & Giedroc, D. P. (2024). Bacterial metallostasis: Metal sensing, metalloproteome remodeling, and metal trafficking. *Chemical Reviews*, *124*, 13574–13659.

Cappuccino, J. G., & Sherman, N. (2014). *Microbiology: A laboratory manual* (10th ed.). Boston: Pearson.

Chakraborty, S., Talukdar, A., Dey, S., & Bhattacharya, S. (2025). Role of fungi, bacteria and microalgae in bioremediation of emerging pollutants with special reference to pesticides, heavy metals and pharmaceuticals. *Discover Environment*, *3*, 91.

Chiaramonte, N., Romanelli, M. N., Teodori, E., & Supuran, C. T. (2018). Amino acids as building blocks for carbonic anhydrase inhibitors. *Metabolites*, 8, 36.

Clarkson, T. W., & Magos, L. (2006). The toxicology of mercury and its chemical compounds. *Critical Reviews in Toxicology*, *36*, 609–662.

Clarridge, J. E. (2004). Impact of 16S rRNA gene sequence analysis for identification of bacteria on clinical microbiology and infectious diseases. *Clinical Microbiology Reviews*, *17*, 840–862.

Dash, H. R., & Das, S. (2012). Bioremediation of mercury and the importance of bacterial *mer* genes. *International Biodeterioration & Biodegradation*, *75*, 207–213.

De, J., Dash, H. R., & Das, S. (2014). Mercury pollution and bioremediation—A case study on biosorption by a mercury-resistant marine bacterium. In Das, S. (Eds.), *Microbial biodegradation and bioremediation* (pp. 137–66). Elsevier.

Delaney, C., Schnell, A., Cammarata, L. V., Yao-Smith, A., Regev, A., Kuchroo, V. K., & Singer, M. (2019). Combinatorial prediction of marker panels from single-cell transcriptomic data. *Molecular Systems Biology*, *15*, e9005.

Esdaile, L. J., & Chalker, J. M. (2018). The mercury problem in artisanal and small-scale gold mining. *Chemistry: A European Journal*, *24*, 6905–6916.

Felsenstein, J. (1985). Confidence limits on phylogenies: An approach using the bootstrap. *Evolution*, *39*, 783.

Fioravanti, R., Muzzioli, L., Maurel, E., Palma, G., Calabrese, G., Angioni, A., Rocca, C. L., Amntovani, A., Pexxana, A., Donini, L. M. (2025). Bioaccumulation and biomagnification of mercury along the seafood chain in Europe: A systematic review. *Foods*, *14*, 3752.

Freedman, Z., Zhu, C., & Barkay, T. (2012). Mercury resistance and mercuric reductase activities and expression among chemotrophic thermophilic *Aquificae*. *Applied and Environmental Microbiology*, *78*, 6568–6575.

Gadd, G. M. (2010). Metals, minerals and microbes: Geomicrobiology and bioremediation. *Microbiology*, *156*, 609–643.

Haferburg, G., & Kothe, E. (2007). Microbes and metals: Interactions in the environment. *Journal of Basic Microbiology*, *47*, 453–67.

Harmoko, D. (2025). Isolation of mercury-resistant bacteria in the Brantas River, Malang, Indonesia. *Svāsthya Trends in General Medicine and Public Health*, *2*, e77.

Harms, H., Schlosser, D., & Wick, L. Y. (2011). Untapped potential: exploiting fungi in bioremediation of hazardous chemicals. *Nature Reviews Microbiology*, *9*, 177–192.

Hillion, M., & Antelmann, H. (2015). Thiol-based redox switches in prokaryotes. *Biological Chemistry*, *396*, 415–444.

Kåhrström, C. T. (2014). Adaptation after jumping ship. *Nature Reviews Microbiology*, *12*, 236–237.

Kempf, B., & Bremer, E. (1998). Uptake and synthesis of compatible solutes as microbial stress responses to high-osmolality environments. *Archives of Microbiology*, *170*, 319–330.

Kim, M., Oh, H. S., Park, S. C., & Chun, J. (2014). Towards a taxonomic coherence between average nucleotide identity and 16S rRNA gene sequence similarity for species demarcation of prokaryotes. *International Journal of Systematic and Evolutionary Microbiology*, *64*, 346–351.

Kumar, A., Solanki, M. K., Kumar, M., Kaushik, A., Arya, A., Saikia, M., Gaur, V. K., Singh, R. P., Singh, S. K., Singh, V. K., & Dufosse, L. (2026). The microbial strategies for the management of chemical pesticides: A comprehensive review. *Current Research in Microbial Science*, *10*, 100519.

Kusuma, J., Analianasari, Wahyudi, A., Abdullah, M. K., Hasan, A. Z., Asrowardi, I, Fitriani, Tahir, M. (2025). Diversity of the non-targeted metabolomic data across various varieties of Cloves (*Syzygium* spp.). *Data Brief* 58, 111237.

Lalucat, J., Bennasar, A., Bosch, R., García-Valdés, E., & Palleroni, N. J. (2006). Biology of *Pseudomonas stutzeri*. *Microbiology and Molecular Biology Reviews*, *70*, 510–547.

Leboffe, M. J., & Pierce, B. E. (2016). *Microbiology: Laboratory theory & application* (3rd ed.). Englewood, CO: Morton Publishing.

Li, T., Fang, Y., Chai, Z., Ji, L., Jiang, Z., Meng, D., He, B., Hu, X., Xi, H., Jia, X., & Li, D. (2025). Cyclic dipeptides from endophytic bacterium *Bacillus velezensis* as potential flavor precursors. *Frontiers in Microbiology*, *16*, 1565502.

Madigan, M. T., Bender, K. S., Buckley, D. H., Sattley, W. M., Stahl, D. A., & Brock, T. D. (2019). *Brock biology of microorganisms* (15th ed.). Pearson.

Mahbub, K. R., Krishnan, K., Naidu, R., & Megharaj, M. (2017). Mercury remediation potential of a mercury resistant strain *Sphingopyxis* sp. SE2 isolated from contaminated soil. *Journal of Environmental Sciences*, *51*, 128–137.

Min, S. J., Kim, J. G., & Baek, K. (2020). Role of carbon fiber electrodes and carbonate electrolytes in electrochemical phenol oxidation. *Journal of Hazardous Materials*, *400*, 123083.

Monod, J. (1949). The growth of bacterial cultures. *Annual Review of Microbiology*, *3*, 371–394.

Nakamoto, K. (2008). Infrared and raman spectra of inorganic and coordination compounds: Part A: Theory and applications in inorganic chemistry (1st ed). Wiley.

Nies, D. H. (1999). Microbial heavy-metal resistance. *Applied Microbiology and Biotechnology*, *51*, 730–750.

Nies, D. H. (2016). The biological chemistry of the transition metal “transportome” of *Cupriavidus metallidurans*. *Metallomics*, *8*, 481–507.

Osborn, A. M., Bruce, K. D., Strike, P., & Ritchie, D. A. (1997). Distribution, diversity and evolution of the bacterial mercury resistance (*mer*) operon. *FEMS Microbiology Reviews*, *19*, 239–262.

Pande, V., Pandey, S. C., Sati, D., Bhatt, P., & Samant M. (2022). Microbial interventions in bioremediation of heavy metal contaminants in agroecosystem. *Frontiers in Microbiology*, *13*, 824084.

Purkan, P., Nurmalyya, S., & Hadi, S. (2016). Resistance level of *Pseudomonas stutzeri* against mercury and its ability in production of mercury reductase enzyme. *Molekul*, *11*, 230.

Pushkar, B., Sevak, P., & Singh, A. (2019). Bioremediation treatment process through mercury-resistant bacteria isolated from Mithi river. *Applied Water Science*, *9*, 117.

Quintero, M., Zuluaga-Valencia, S. D., Ríos-López, L. G., Sánchez, O., Bernal, C. A., Sepúlveda, N., Gomez-Leon, J. (2024). Mercury-resistant bacteria isolated from an estuarine ecosystem with detoxification potential. *Microorganisms*, *12*, 2631.

Rodiansyah, A., Mahmudah, A. F., Ulfah, M. M., Rohmawati, U., Listyorini, D., Suyono, E. A., Prabaningtyas, S. (2021). Identification of potential bacteria on several lakes in East Java, Indonesia based on 16S rRNA sequence analysis. *HAYATI Journal of Biosciences*, *28*, 136.

Rohmawati, U., & Kasiamdari, R. S. (2022). Morphological, molecular characterization, and physico-chemical analysis of *Trichoderma yunnanense* as indigosol golden yellow dye-decolorizing fungus. *The Philippine Journal of Science*, *151*, 6B.

Rosselló-Móra, R., & Amann, R. (2015). Past and future species definitions for Bacteria and Archaea. *Systematic and Applied Microbiology*, *38,* 209–216.

Rytuba, J. J. (2003). Mercury from mineral deposits and potential environmental impact. *Environmental Geology*, *43*, 326–338.

Schafer, F. Q., & Buettner, G. R. (2001). Redox environment of the cell as viewed through the redox state of the glutathione disulfide/glutathione couple. *Free Radical Biology and Medicine*, *30*, 1191–1212.

Shamim, S. (2018). Biosorption of heavy metals. In Derco, J., & Vrana, B. (Eds.), *Biosorption*. InTech.

Sleator, R. D., & Hill, C. (2002). Bacterial osmoadaptation: The role of osmolytes in bacterial stress and virulence. *FEMS Microbiology Reviews*, *26*, 49–71.

Tang, H., Xiang, G., Xiao, W., Yang, Z., & Zhao, B. (2024). Microbial mediated remediation of heavy metals toxicity: Mechanisms and future prospects. *Frontiers in Plant Science*, *15*, 1420408.

Telmer, K. H., & Veiga, M. M. (2009). World emissions of mercury from artisanal and small scale gold mining. In Mason, R., & Pirrone, N. (Eds.). *Mercury fate and transport in the global atmosphere* (pp. 131–172). Springer.

Timková, I., Maliničová, L., Nosáľová, L., Kolesárová, M., Lorková, Z., Petrová, N., Pristas, P., & Kriskova, J. (2024). Genomic insights into the adaptation of *Acinetobacter johnsonii* RB2-047 to the heavy metal-contaminated subsurface mine environment. *BioMetals*, *37*, 371–387.

Tromas, N., Taranu, Z. E., Castelli, M., Pimentel, J. S. M., Pereira, D. A., Marcoz, R., Shapiro, B. J., Giani, A. (2020). The evolution of realized niches within freshwater *Synechococcus*. *Environmental Microbiology*, *22*, 1238–1250.

Upadhyay, K. H., Vaishnav, A. M., Tipre, D. R., Patel, B. C., & Dave, S. R. (2017). Kinetics and mechanisms of mercury biosorption by an exopolysaccharide producing marine isolate *Bacillus licheniformis*. *3 Biotech*, *7*, 313.

Veglio’, F., & Beolchini, F. (1997). Removal of metals by biosorption: A review. *Hydrometallurgy*, *44*, 301–316.

Volesky, B. (2007). Biosorption and me. *Water Research*, *41*, 4017–4029.

Wang, Y., & Greger, M. (2004). Clonal differences in mercury tolerance, accumulation, and distribution in willow. *Journal of Environmental Quality*, *33*, 1779–1785.

Wang, J., & Chen, C. (2009). Biosorbents for heavy metals removal and their future. *Biotechnology Advances*, *27*, 195–226.

Wang, L., Hou, D., Cao, Y., Ok, Y. S., Tack, F. M. G., & Rinklebe, J., (2020). et al. Remediation of mercury contaminated soil, water, and air: A review of emerging materials and innovative technologies. *Environment International*, *134*, 105281.

Weisburg, W. G., Barns, S. M., Pelletier, D. A., & Lane, D. J. (1991). 16S ribosomal DNA amplification for phylogenetic study. *Journal of Bacteriology*, *173*(2), 697–703.

Windarsih, A., Suratno, Warmiko, H. D., Indrianingsih, A. W., Rohman, A., & Ulumuddin, Y. I. (2022). Untargeted metabolomics and proteomics approach using liquid chromatography-Orbitrap high resolution mass spectrometry to detect pork adulteration in *Pangasius hypopthalmus* meat. *Food Chemistry*, *386*, 132856.

Yao, H., Wang, H., Ji, J., Tan, A., Song, Y., & Chen, Z. (2023). Isolation and identification of mercury-tolerant bacteria LBA119 from molybdenum-lead mining soils and their removal of Hg^{2+}. *Toxics*, *11*, 261.

Zheng, R., Wu, S., Ma, N., & Sun, C. (2018). Genetic and physiological adaptations of marine bacterium *Pseudomonas stutzeri* 273 to mercury stress. Frontiers in Microbiology, 9, 682.